Engineering Structures 346 (2026) 121622

Contents lists available at ScienceDirect

Engineering Structures

journal homepage: www.elsevier.com/locate/engstruct

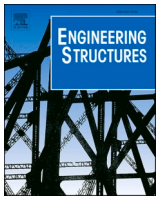

A genetic algorithm-based calibration procedure for hysteresis loops in timber structures

Hoang D. Nguyen *, Qipei Mei, Ying Hei Chui

Department of Civil and Environmental Engineering, Faculty of Engineering, University of Alberta, Edmonton, Alberta T6G 1H9, Canada

ARTICLE INFO

Keywords:
Hysteresis behavior
Timber structures
Genetic algorithm
Calibration procedure
Optimization
HystereticSM material model

ABSTRACT

Hysteresis loops of timber structures often exhibit complex behaviors such as pinching and stiffness degradation, which are challenging to model accurately. This study proposes an automated calibration procedure for hysteresis loops of timber components and systems using the *HystereticSM* material model in OpenSees combined with a genetic algorithm (GA). The *HystereticSM* model was selected for its ability to capture pinching, strength, and stiffness degradation while requiring relatively few input parameters, thereby simplifying the calibration process. In the proposed framework, GA optimization is employed with energy dissipation as the objective function to efficiently match experimental hysteresis behavior. To demonstrate the robustness of the proposed procedure, it was applied to the calibration of timber connections fabricated with three types of fasteners (timber rivet, bolt, and nail) and a light wood-frame shear wall. Results showed that the calibrated models reproduced the experimental hysteresis loops with small errors in both peak force and energy dissipation, confirming the effectiveness of the approach across different hysteresis characteristics. In addition, practical guidelines for parameter initialization and recommendations for the calibration process are provided, supporting broader application of the framework. These findings highlight the potential of the proposed procedure as a standardized and efficient approach for calibrating hysteresis models of timber structures and establish a foundation for extending it to other different hysteresis characteristics in future work.

1. Introduction

Timber offers a sustainable alternative for building construction, addressing the urgent demand for environmentally responsible and efficient material use [1–3]. In the context of climate change, such practices are not only economically beneficial but also critical for long-term resilience. Structural timber, a renewable resource, is abundantly available and has a smaller environmental footprint compared to other construction materials [4–6].

To promote the broader use of structural timber in real-world applications, the behavior of timber connections and systems must be thoroughly investigated, especially given that recent studies [7,8] indicate connection failures have contributed to nearly 25 % of timber structure collapses. While numerous studies have experimentally investigated the behavior of timber structures [9–12] such tests are costly and limited to specific configurations or small-scale components. Numerical models thus provide an essential complement, enabling the study of larger systems and parametric variations at lower cost. To overcome this limitation, numerical models have been employed to enable further investigation, such as analyzing taller timber buildings or examining the use of timber connections within entire structural systems. To develop a reliable numerical model, the nonlinear behavior of timber connections or components used in the numerical models is typically calibrated based on their responses observed in experimental tests. To incorporate this into numerical simulations, spring elements are commonly used to simulate the nonlinear behavior in timber connections or systems. Compared to the mechanistic method, it is simpler, requires less computational effort, and is well-suited for parametric analyses. For developing numerical models, OpenSees [13] is among the widely used software tools in the field of structural engineering [14–17] and has become increasingly common in timber structure research and design since it provides versatile options for modeling nonlinear material behavior [18]. Two widely used models in OpenSees for timber connections are SAWS [19,20] and Pinching4 [21]. Both can simulate key behaviors such as the backbone curve, pinching effects, and strength and stiffness degradation. Numerous studies have investigated the behavior of timber structures by calibrating these material models using experimental data. For instance, Shen et al. [22] calibrated both the

* Corresponding author.
E-mail address: dachoang@ualberta.ca (H.D. Nguyen).

https://doi.org/10.1016/j.engstruct.2025.121622
Received 13 May 2025; Received in revised form 5 September 2025; Accepted 16 October 2025
Available online 22 October 2025

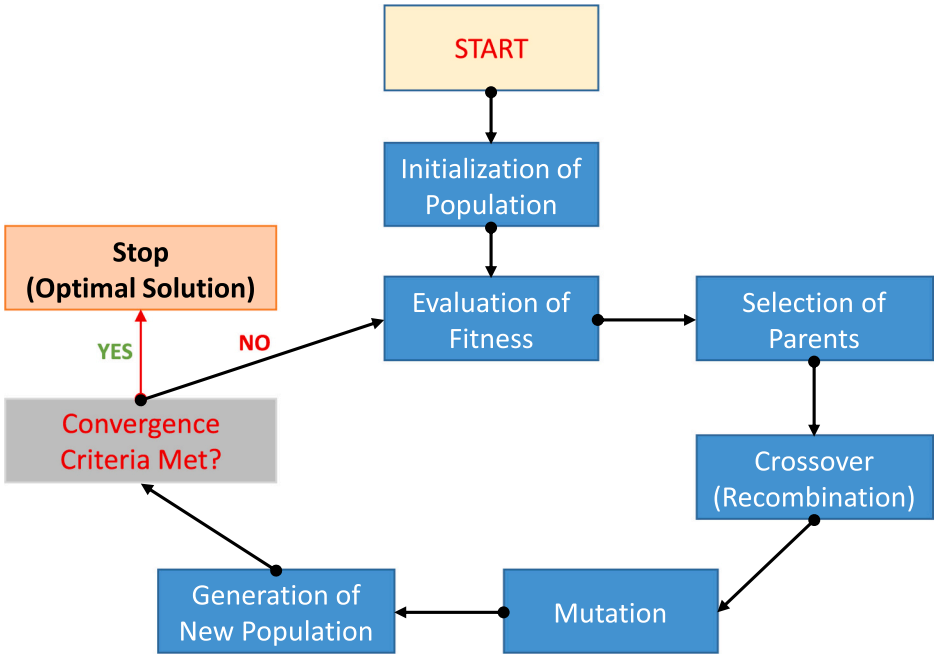

Fig. 1. Main concept of GA.

SAWS and Pinching4 models to simulate the static monotonic and cyclic behavior of bracket connections in cross-laminated timber (CLT) shear walls. The results indicated that both models were capable of capturing pinching behavior as well as strength and stiffness degradation. Specifically, the Pinching4 model demonstrated better performance than the SAWS model in representing these nonlinear characteristics. Schneider et al. [23] developed a numerical model of CLT mechanical connections based on the SAWS model to evaluate their performance under cyclic loading. Cao et al. [24] used the SAWS and Pinching4 models to calibrate timber–concrete bolted connections under cyclic loading. The authors reported that the simulated hysteresis curves from both models showed good agreement with the experimental data.

Morshedi et al. [25] examined the seismic force modification factors related to the overstrength and ductility of light wood-frame shear walls. Their numerical model, developed in OpenSees, used the Pinching4 material model calibrated by adjusting various parameters to closely match experimental data from shear wall tests. Jerves and Phillips [26] developed a numerical model for CLT rocking walls with modular base connections and laminated strand lumber wall toes using OpenSeesPy [27], and compared the results with those from experiments. Chen et al. [28] used the Pinching4 model to calibrate the cyclic behavior of angle brackets and hold-downs, which were used to investigate the seismic response of CLT shear walls. Additional studies of hysteretic responses can be found in the literature [29,30].

The literature reviewed above demonstrates that both the calibrated numerical models are capable of simulating the cyclic behavior of timber connections and components observed in the experiments, making them suitable for in-depth investigations into the behavior of timber systems. However, the SAWS model is limited in that it cannot capture asymmetrical envelope behavior [31], as it only supports symmetrical responses. In addition, the SAWS model experiences convergence issues during nonlinear time history analysis. In contrast, the Pinching4 material model addresses this limitation by allowing separate input of load-displacement values for the positive and negative response envelopes. Despite this advantage, the Pinching4 model includes 39 input variables, with 23 parameters specifically related to pinching, damage, and degradation. This large number of parameters makes the calibration process challenging. In particular, identifying suitable initial values for these 23 parameters that can be generally applied across various hysteresis characteristics in cyclic behavior remains a significant difficulty in the calibration process. Therefore, as shown in the literature reviewed above, most studies typically focused on calibrating only one type of timber connection or component. In other words, the calibration has not been applied to a variety of hysteresis characteristics.

Recently, Mazzoni [32] has extended the original *Hysteretic* material model in OpenSees [13] to create *HystereticSM*, which offers greater flexibility in simulating hysteresis behavior. This model is also capable of capturing pinching effects, as well as strength and stiffness degradation. *HystereticSM* model requires fewer input parameters related to pinching, damage, and degradation compared to Pinching4 (7 versus 23), while at the same time it allows users to provide more load–displacement data points (up to seven rather than four) to define the backbone envelope, which can further facilitate the calibration process. It should be noted that *HystereticSM* still permits the use of only four points when the hysteresis loop is relatively simple. This flexibility enables a more accurate representation of envelope curves when hysteresis loops exhibit multiple turning points or nonlinear characteristics. A further motivation for this study is to introduce *HystereticSM* as a viable alternative for modeling the hysteretic behavior of timber structures effectively. In fact, although the *HystereticSM* model requires fewer input parameters, an automated calibration process is still necessary due to the number of parameters that must be tuned, which can make manual calibration time-consuming.

It is also worth noting that despite the widespread use of material model calibration in timber engineering research, a complete and standardized calibration procedure, which can be used for different experimental results, has yet to be established. To address these gaps, this study proposes an automated calibration framework that combines the *HystereticSM* model with a genetic algorithm (GA). The GA optimizes model parameters to replicate experimental hysteresis loops based on energy dissipation, offering a standardized and efficient calibration procedure applicable to different timber connections and systems. GA has been widely used in optimization tasks to handle complex, multi-dimensional, and nonlinear problems [33,34]. For example, Si et al. [35] calibrated the Pinching4 model using GA to investigate the cyclic behavior of laminated veneer lumber and glued laminated bamboo connections with slotted-in steel plates. Dong et al. [36] employed GA to calibrate the DowelType model for timber joints. Wei and Su [37]

successfully calibrated a modified Bouc–Wen model using GA. In this study, GA is employed to efficiently optimize input parameters that allow the HystereticSM model to replicate the hysteresis loop observed in experiments, with the difference in energy dissipation used as the objective function. The introduction of an automated and integrated calibration procedure, combined with the application of a new material model for calibration, highlights the novelty of this study. The proposed procedure is then applied to calibrate hysteresis loops for different types of fasteners in timber connections and light wood-frame shear walls. The outcomes of these applications illustrate the effectiveness of the proposed approach for automating the calibration of numerical models for timber components and systems, along with guidance and recommendations in the calibration process.

2. Research background

2.1. Genetic algorithm

Genetic Algorithm (GA) [38] is an optimization method that is used to determine the best possible solution for a given computational problem by maximizing or minimizing a specific objective function. GA is classified as an adaptive heuristic search technique and is one of the components of evolutionary algorithms [39]. It is inspired by the principles of natural selection and genetics, employing a combination of random search and historical data to efficiently explore solution spaces and converge toward the optimal solution. GA operates by simulating natural evolutionary processes, which means those species that can adapt to changes in their environment can survive, reproduce, and go to the next generation. Therefore, GA is extensively applied to tackle complex optimization and search problems by efficiently generating high-quality solutions, especially in cases where conventional methods face limitations.

Fig. 1 shows the main concept of GA. Initially, a diverse population of potential solutions is created, each encoded in a structured format known as a chromosome (also known as the solution), typically represented as binary strings, real-valued vectors, or permutations, depending on the nature of the optimization problem. In this study, the chromosome is a real-valued vector consisting of the input parameters for the *HystereticSM* material model. The algorithm then evaluates the fitness of each individual parameter using a specifically designed fitness function, defined as the cumulative energy error between the simulated and experimental hysteresis loops. The dissipated energy of each loop is computed as the enclosed area of the force–displacement curve using trapezoidal numerical integration. The cumulative energy error is expressed as the relative difference between the simulated and experimental energies, and the objective of the optimization is to minimize this error, ensuring that the calibrated model closely matches the energy dissipation observed in the experiments. Based on these fitness scores, a parent selection mechanism is applied in which individuals with higher fitness values are assigned proportionally greater probabilities of being chosen for reproduction. This preferential selection ensures that fitter individuals contribute more frequently to the next generation. At the same time, because the selection is probabilistic (roulette wheel selection), less-fit individuals still retain a nonzero chance of being selected, which helps maintain population diversity and prevents premature convergence. The selected parents then undergo crossover (recombination), where pairs of parent chromosomes exchange genetic information to create offspring (also known as the new trial solution) that combine desirable traits from both parents. This mechanism promotes the exploration of new regions within the solution space and increases the likelihood of discovering improved solutions. Next, mutation is applied by randomly altering one or more components of a chromosome, further enhancing genetic diversity and reducing the risk of the algorithm becoming trapped in local optima.

After the mutation step, the algorithm proceeds with the generation of a new population, where the offspring produced through crossover and mutation form the updated population for the next iteration. Once the new population is generated, the algorithm checks whether the convergence criteria have been met. These criteria typically include reaching the maximum number of generations, achieving a predefined fitness threshold, or observing no significant improvement in fitness values over multiple iterations. In this study, the maximum number of generations is used as the convergence criteria to stop the process. If the convergence criteria are not satisfied, the algorithm returns to the evaluation of fitness step, ensuring that the new population is assessed and undergoes subsequent iterations of selection, crossover, and mutation. This iterative process continues until the stopping condition is met. Once convergence is achieved, the algorithm terminates, and the best solution found is returned as the optimal solution.

In this study, the package known as *geneticalgorithm* in python [40] was used for the optimization process. Every evolutionary algorithm requires certain parameters to be adjusted for optimal performance. GA implemented in *geneticalgorithm* package also requires several key parameters that influence its efficiency and solution quality. The parameters along with their descriptions are presented in Appendix A. Detailed information of the used package and the theory of GA can be found in the literature [41,42].

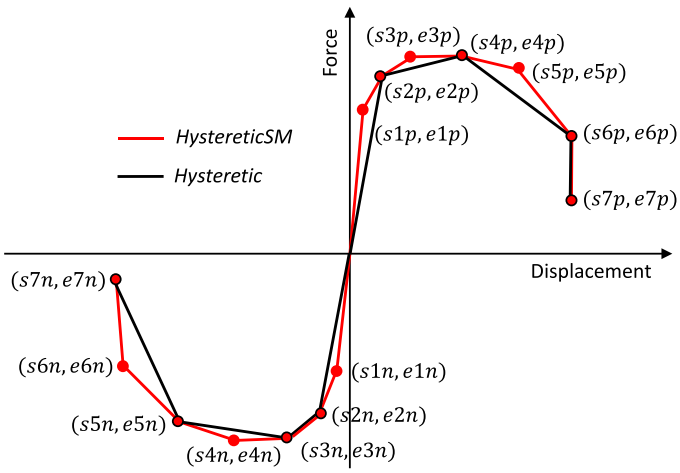

Fig. 2. Backbone curves for HystereticSM and Hysteretic material models.

2.2. HystereticSM material model

In this study, *HystereticSM* material model was employed to calibrate the cyclic hysteresis behavior observed in experimental tests. *HystereticSM* model, recently developed as an extension of the Hysteretic model in OpenSees [27], is a uniaxial multilinear hysteretic model capable of simulating pinching effects in force and deformation, damage accumulation related to ductility and energy dissipation, and stiffness degradation during unloading based on ductility levels. Fig. 2 illustrates the visualization of the backbone curve for the *HystereticSM* and Hysteretic material models. Building on the original Hysteretic material, which permits inputting four pairs of force–displacement (or stress–-strain, moment–rotation, or moment–curvature) values, HystereticSM retains this compatibility while also allowing users to specify up to seven pairs when a more detailed backbone curve is required to fully capture the hysteresis behavior. As shown in Fig. 2, this flexibility enables a more accurate representation of envelope curves when hysteresis loops exhibit multiple turning points or nonlinear characteristics, while still permitting the simpler four-point definition when appropriate. Furthermore, the number of segments in the monotonic envelope can be increased (up to seven) to better capture nonlinear response, while retaining the option of four segments ensures backward compatibility with the original Hysteretic model. This added flexibility also aligns with the backbone curve definitions specified in ASCE-41 [43].

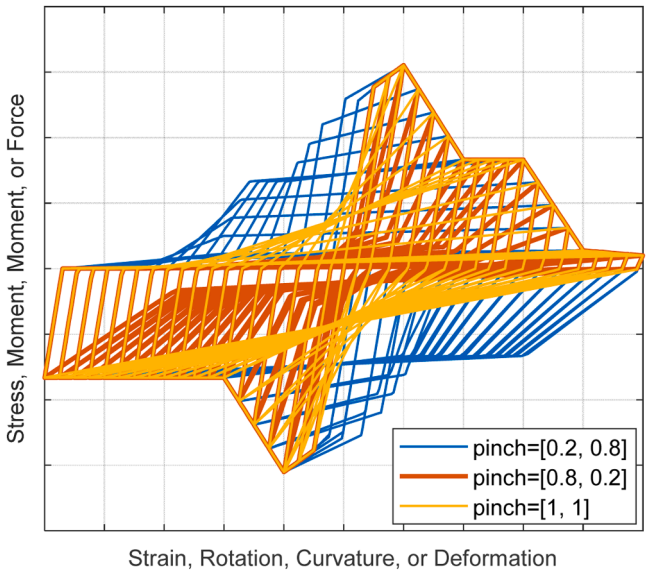

Fig. 3. Parametric study on pinching parameters of HystereticSM.

Furthermore, the force–displacement values can be independently defined for positive and negative loading directions, making the model particularly advantageous for capturing asymmetrical envelope behavior. During optimization, the ability to accommodate multiple data points (i.e., seven points in each direction) and separately define the envelope for positive and negative loading directions allows the GA to efficiently calibrate material parameters to closely align with experimental results.

Additionally, another essential input parameter that enables modelers to simulate crack opening and closing during cyclic loading of connections or structural members is the parameter controlling the pinching effect. The pinching effect in a hysteresis loop describes the narrowing of the loop in the middle during cyclic loading, typically caused by mechanisms such as slip, cracking, or degradation of material interfaces. This characteristic shape indicates a reduction in effective stiffness and a significant loss of energy dissipation capacity. In the *HystereticSM* material, the pinching effect is captured through the parameters $pinchx and $pinchy. The parameter $pinchx controls the degree of pinching along the displacement axis during unloading and reloading, while $pinchy governs the pinching along the force axis. Lower values of $pinchx and $pinchy produce narrower loops with pronounced inward pinching, whereas values closer to 1 maintain fuller loops with limited pinching. Fig. 3 demonstrates the variations in hysteresis behavior corresponding to different values of $pinchx and $pinchy. It is evident that these parameters significantly influence the shape and characteristics of the hysteresis loop. In other words, this shows the advantage of this material to be able to simulate various pinching behaviors under cyclic loading.

Moreover, three parameters— $damage, $beta, and $degEnv—are available to represent cyclic strength and stiffness degradation. Specifically, the $damage parameter captures the damage effects related to ductility and energy dissipation, $beta defines stiffness degradation during unloading based on ductility, and $degEnv controls the degradation of the positive and negative envelope curves. It should be noted that these three damage parameters are optional, with default values set to zero. Summarization of the six primary input parameters for the *HystereticSM* material, along with brief descriptions are provided in Appendix B. Detailed information about the *HystereticSM* material model as well as the parametric studies on $damage, $beta, and $degEnv can be found in the literature [32] and in the OpenSees documentation for *HystereticSM* uniaxial material model [13].

3. Proposed procedure for calibration of *HystereticSM* using genetic algorithm

In this study, a novel procedure, illustrated in Fig. 4, is proposed for calibrating the input parameters of the *HystereticSM* material model based on experimental data using the GA. For the initial information required in the procedure, the steps within the GA and its input parameters were introduced in Section 2.1. Meanwhile, the loading protocol was obtained directly from testing, as it was recorded during the experiment.

The final input information, which includes the initial values and parameter boundaries of the *HystereticSM* model, plays a crucial role in this procedure. These input parameters are sent to the OpenSees model to generate a hysteresis loop, which is then compared with the experimental results. Accordingly, selecting suitable starting points can significantly reduce the computational cost of the optimization process. In other words, the closer the initial values are to the optimal solution, the less effort is required to find the optimal parameters. Therefore, this study introduces a general approach for determining appropriate initial load and displacement values from the experiments. This approach aims to eliminate the need for manual selection. Specifically, based on experimental data, the alpha shapes theory [44], which generalizes the concept of a convex hull to allow for concave boundaries, is utilized to

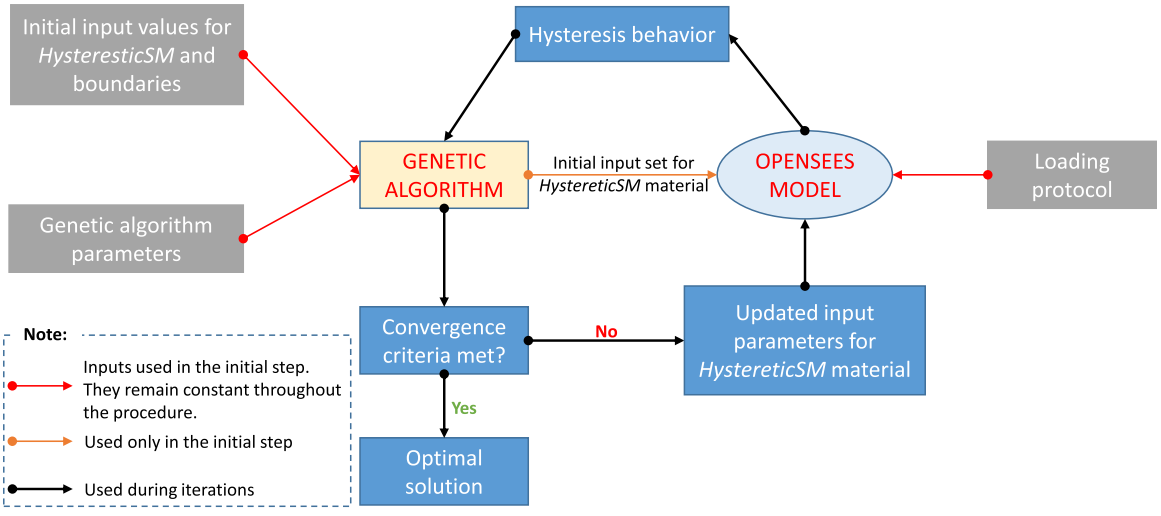

Fig. 4. Calibration procedure for HystereticSM using GA.

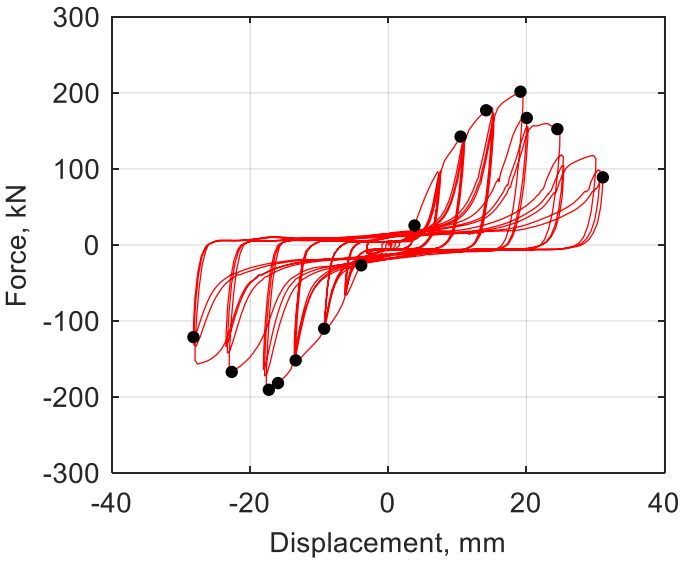

Fig. 5. Example of estimated load-displacement values.

accurately capture the envelope of the hysteresis loop. The identified boundary is then divided into two distinct segments representing the negative and positive sides. A polynomial fitting procedure is applied to the boundary data to smooth the curve and facilitate precise selection of representative points. The main reason for applying polynomial fitting is that, in some cases, the number of points determined by the alpha shapes theory is fewer than seven, while in other cases, the boundary may be excessively smooth with too many points. In this study, a polynomial of degree four was used for this fitting process. Since the displacement (or strain) values must be unique in the *HysteresticSM* material model, unique displacement values are carefully identified and selected. Seven evenly spaced data points, including the peak points, are chosen for both negative and positive sides. After identifying these boundary points, each selected point is matched and replaced with the closest corresponding point from the original experimental dataset using Euclidean distance [45]. Moreover, the *HysteresticSM* material model requires strictly monotonic displacement points (i.e., increasing on the positive side and decreasing on the negative side). To prevent errors during optimization, slight numerical adjustments are introduced when displacement values are too close to each other. The magnitude of these adjustments depends on the user-defined upper and lower bounds of each parameter, which must be specified in the initial step. For example, if bounds of ±5 % are applied, the adjustment procedure ensures that the difference between any two consecutive strain values in the initial input is greater than 10 %. Finally, the resulting boundary points, which represent a precise yet simplified characterization of the cyclic behavior, are structured appropriately and are ready for immediate use in the optimization process. It is noted that the above procedure may not be effective for all types of hysteresis loops. In such cases, manual parameter selection should be employed. Fig. 5 presents an example of estimated seven pairs of load-displacement values for both the positive and negative sides of an experimental test using the proposed approach.

Table 1
Selected input parameters for GA.

Parameter	Value
'max_num_iteration'	1000
'population_size'	10
'mutation_probability'	0.1
'elit_ratio'	0.01
'crossover_probability'	0.5
'parents_portion'	0.3
'crossover_type'	"uniform"
'max_iteration_without_improv'	50

For the pinching parameters, as discussed in Section 2.2, these parameters significantly influence the shape and characteristics of the hysteresis loop. Fig. 3 illustrates how the shape changes under three different pinching parameter cases. Generally, there is no established method for automatically selecting the initial values of the pinching parameters. Therefore, to enhance efficiency, it is recommended that these parameters should be selected based on different hysteresis loop shapes, using the reference values provided in Fig. 3. It is noted that the random values with a large upper and lower range could be used. However, this approach may increase computational cost. For the parametric study of other parameters ($damage, $beta, and $degEnv), the information is provided in the OpenSees documentation for *HysteresticSM* material model [13].

Another important information for the optimization process of GA is the objective function. In this procedure, the objective function is the difference in energy dissipation between the hysteresis loops obtained from the test and the numerical model. Specifically, energy dissipation is calculated as the area under the curve. In this study, the loop area was computed using the trapezoidal rule applied to the time-ordered force–displacement pairs. Ultimately, the last information, which is the convergence criteria to stop the GA, was introduced in Section 2.1. The entire procedure can be summarized as follows:

Step 1 - Estimate Initial Load-Displacement Values: Determine the initial values for the seven pairs of load-displacement relationships using the approach introduced earlier.

Step 2 - Estimate Initial Pinching, Beta, Damage, and Degradation Parameters: Select initial pinching, beta, damage, and degradation values based on the shape of the experimental hysteresis loop.

Step 3 - Define Boundary Values: Set the upper and lower limits for the input parameters.

Step 4 - Build the OpenSees Model: Develop an OpenSees model with a single-degree-of-freedom system incorporating a nonlinear zero-length spring using the *HysteresticSM* material. The applied force follows the displacement protocol from the test.

Step 5 - Set GA Parameters: Define the necessary input parameters for the GA, which are introduced in Appendix A.

Step 6 - Run Analysis and Adjust Iterations: Generate material input parameters using the GA based on the initial estimates and their predefined boundaries. These inputs are sent to the OpenSees model, which simulates the hysteresis loop. The simulated response is compared with the experimental results using an objective function (e.g., minimizing the difference in energy dissipation). The GA evaluates whether the stopping criteria are met. If not, it generates a new set of input parameters. This iterative process continues until the convergence criteria are satisfied.

Step 7 - Obtain Optimized Parameters: Complete the process and extract the optimized parameter values for further analysis.

4. Application of calibration procedure to timber components and systems

To demonstrate the robustness of the proposed procedure, it was applied to calibrate the hysteresis loops obtained from testing of timber connections and wood-frame shear walls. Following the steps outlined in Fig. 4 and Section 3, the general input information for the proposed procedure was determined. The parametric study on the pinching parameters affecting the shape of the hysteresis loops was presented in Section 2.2, while the parametric studies of the other parameters are provided in the OpenSees documentation for *HysteresticSM* uniaxial material model [13]. Based on the shape of the hysteresis loops of the considered timber connections and light wood-frame shear wall, the initial values for the pinching parameters were set to 0.8 for $pinchx and 0.2 for $pinchy (Step 2). The values of $damage1, $damage2, $beta, $degEnvP, and $degEnvN were initialized at 0.001. Since the load–displacement values are obtained directly from experimental data,

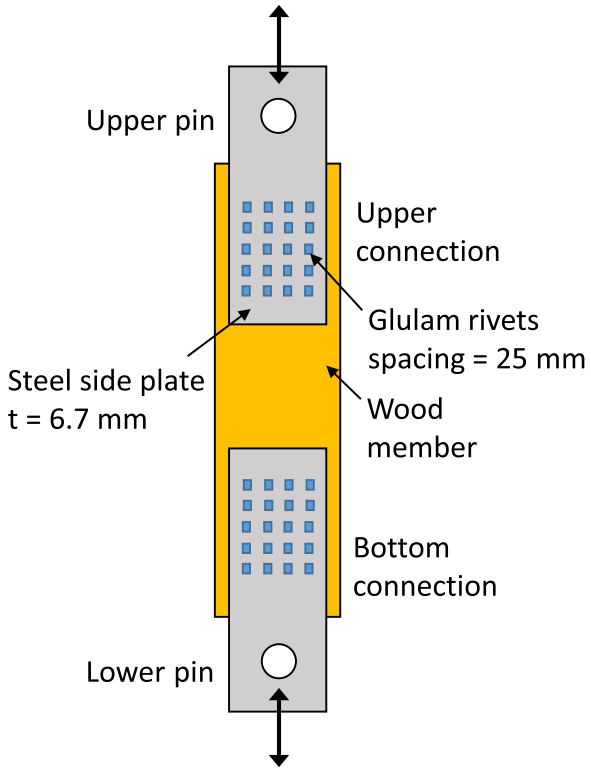

Fig. 6. Configuration of the riveted connections tested by Popovski [46].

a ± 5 % variation was used for their upper and lower bounds (Step 3). It is recommended that the bounds for load–displacement remain small, as they are derived directly from experimental measurements. By contrast, a wider ±50 % variation was applied to the pinching, beta, damage, and degradation parameters to allow a broader search range and improve the ability to match different hysteresis behavior. The initial values for the genetic GA parameters (Step 6) are summarized in Table 1. It is noted that these values are recommended in the *geneticalgorithm* package [40]. The information for the other steps is determined based on each specified experimental test.

Given the initial information, the optimized procedure is applied to timber connections fabricated with three types of fasteners (timber rivet, bolt, and nail) and a light wood-frame shear wall to evaluate its performance, as detailed in the following sections.

4.1. Riveted connection

For this investigation, data from testing of two riveted connections in spruce-pine glulam members of grade 20f-EX [46] were considered. Both connections used 20 timber rivets (4 rows of 5) on each side of the glulam member, for a total of 40 rivets at each end of the glulam member. These two connections were identical except for the length of timber rivets. The connection with shorter rivets (40 mm) is referred to as RC1, while the one with a length of 65 mm is referred to as RC2. The connection specimen configurations are illustrated in Fig. 6.

As required in Step 1, initial load-displacement values are needed. Fig. 7a and Fig. 7b show the selected load-displacement values in both the positive and negative directions for RC1 and RC2, respectively, using the proposed approach described in Section 3.

As described in Step 4, the displacement protocol from the test is required for the OpenSees model. Fig. 8a and Fig. 8b present the displacement protocols used in the experiments for RC1 and RC2, respectively.

All necessary inputs for the calibration are prepared. After running the calibration procedure, the results were obtained. Fig. 9 illustrates the performance of the proposed procedure for the RC1 case. It can be seen that the backbone curve of the hysteresis loop obtained from the simulation is generally close to that obtained from the experiment. As shown in Fig. 9a, the maximum and minimum loads obtained from the numerical model are 107.49 kN and 115.61 kN, respectively, with differences of 0.22 % and 0.42 % compared to the experimental results. These small discrepancies highlight the importance of selecting appropriate initial points for the envelope of the hysteresis loop. In addition, based on the hysteresis loop, the energy dissipation was calculated for both the simulation and the experiment. The energy dissipation from the simulation is 7,575.58 kJ, which is similar from the experiment (7,575.57 kJ). The energy dissipations of simulation and experiment are identical, as demonstrated in Fig. 9b.

The calibration process of the hysteresis loop for the RC2 connection is presented in Fig. 10. As observed, the proposed procedure yields a hysteresis loop that closely matches the experimental results. Fig. 10b indicates that there is a very minimal difference in energy dissipation between the experiment and simulation. Specifically, the energy dissipation measured in the experiment is 16,482.76 kJ, while the simulation produces 16,482.77 kJ. In terms of maximum load, the experiment records 143.72 kN, compared to 143.26 kN in the simulation, corresponding to a discrepancy of 0.32 %. For the negative load region, the values are 149.87 kN in the experiment and 151.31 kN in the simulation, with a difference of 0.96 %.

The rate of convergence to the final results in the calibration procedure for the two rivet connections is presented Fig. 9b and Fig. 10b

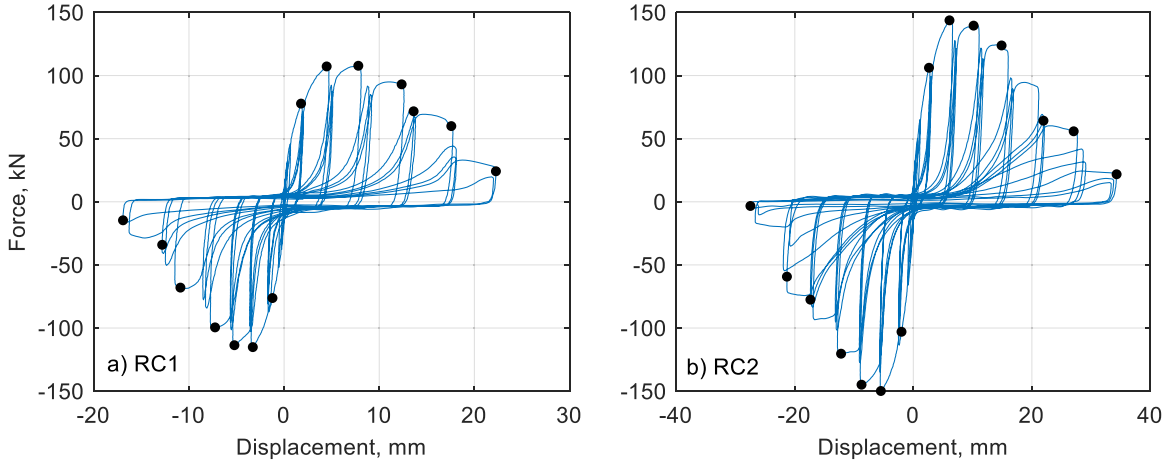

Fig. 7. Selected envelope points of force–displacement curve for riveted connections.

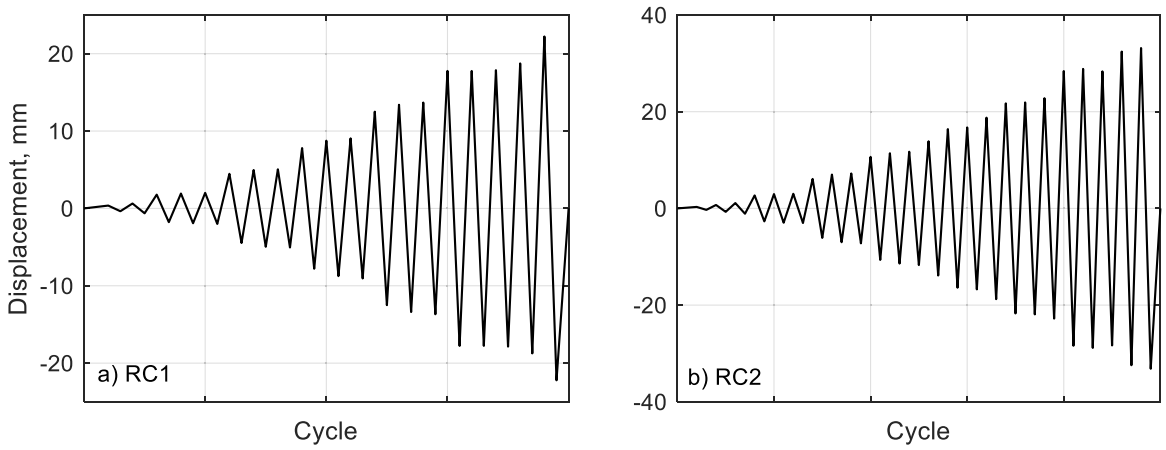

Fig. 8. Displacement protocols used in the experiments for (a) RC1 and b) RC2 connections.

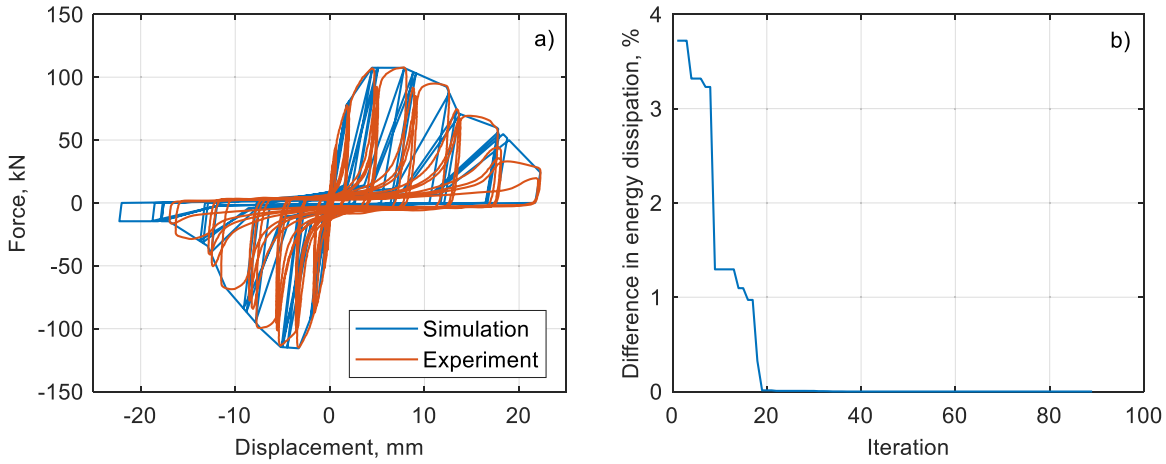

Fig. 9. Performance of the calibration procedure for RC1 connection.

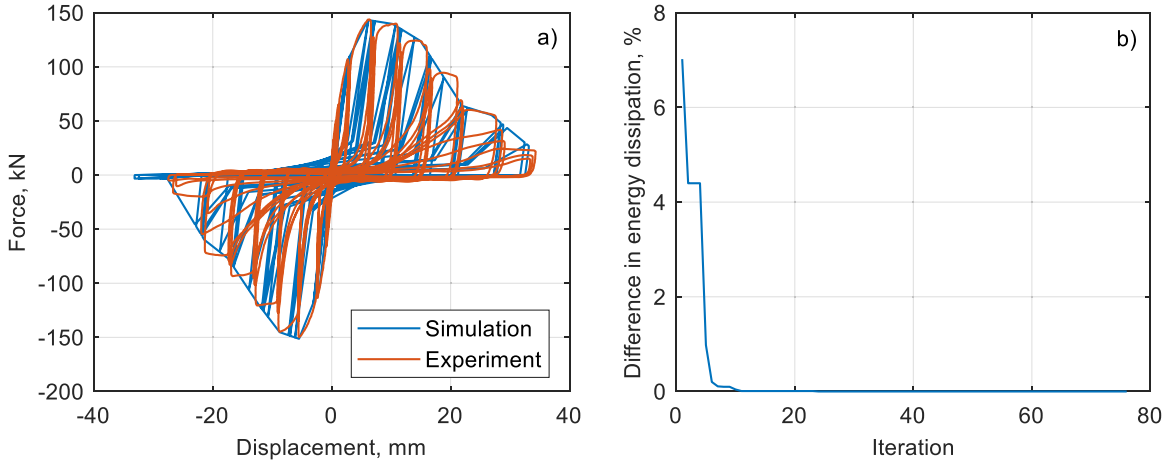

Fig. 10. Performance of the calibration procedure for RC2 connection.

respectively. For the RC1 connection, the GA procedure reaches convergence after 89 iterations, while for RC2, convergence is achieved after 76 iterations.

4.2. Bolted connection

In this assessment, the hysteresis loops of two bolted connections tested by [47] were selected for calibration. These connections consisted of Douglas Fir-Larch glulam member of grade 16c-E. One is a standard bolted connection with four 9.5 mm diameter bolts, referred to as BC1. The other also has four 9.5 mm diameter bolts but includes additional reinforcement using four fully penetrated 8 mm diameter self-tapping screws, referred to as BC2. The details of these connections are shown in Fig. 11.

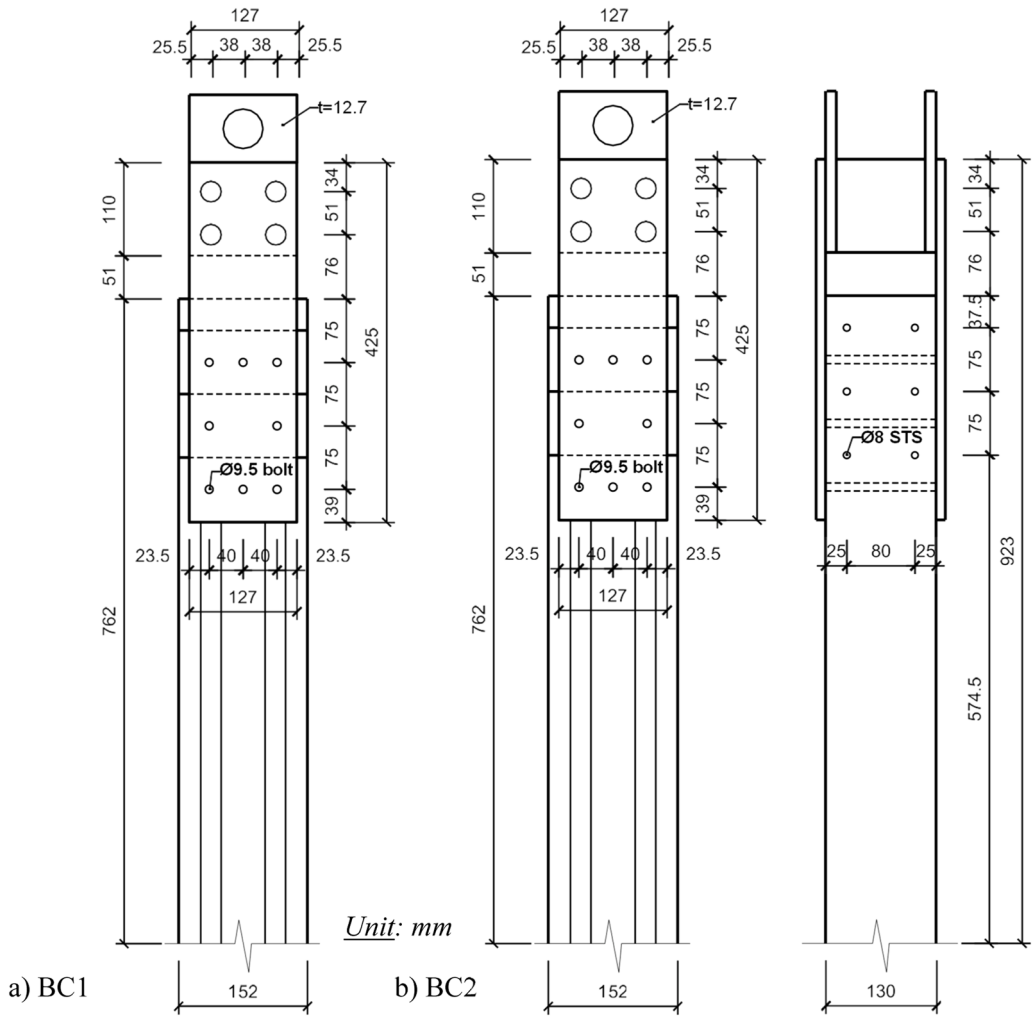

Fig. 11. Specimen configurations of bolted connections [47].

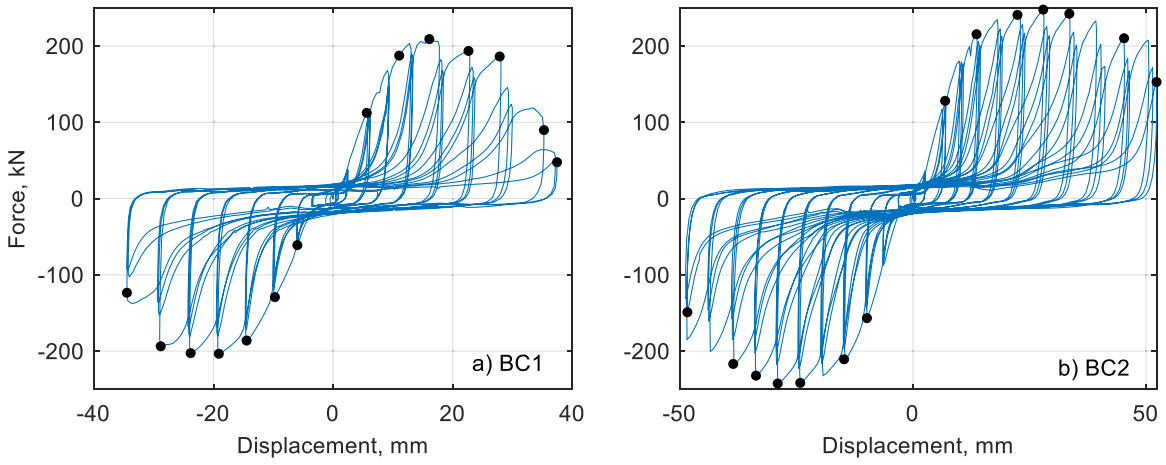

Fig. 12. Selected envelope points of force-displacement curve for bolted connections.

Fig. 12a and Fig. 12b show the selection of envelope values in both positive and negative directions for the BC1 and BC2 connections, respectively. In addition, the two displacement protocols used in these experiments are presented in Fig. 13.

Fig. 14a and Fig. 15a show the hysteresis loops obtained using the proposed procedure for the BC1 and BC2 connections, respectively, along with the corresponding optimization processes presented in Fig. 14b and Fig. 15b. In terms of peak force, the difference on the positive side for BC1 is 0.19 %, while the difference on the negative side is 0.16 %. For BC2, the differences are 0.13 % and 0.96 % on the positive and negative sides, respectively. These small discrepancies indicate that the proposed procedure effectively calibrates the input parameters of

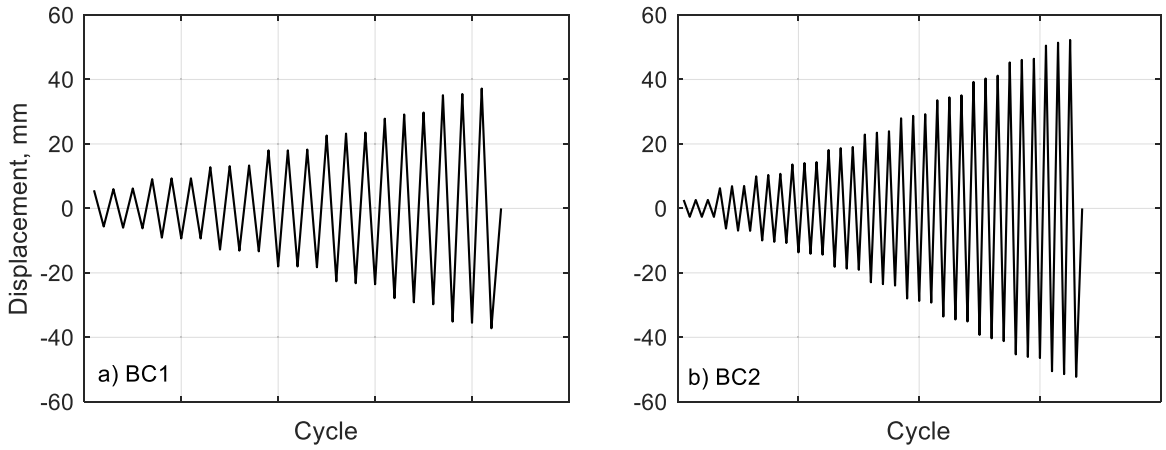

Fig. 13. Displacement protocols used in the experiments for a) BC1 and b) BC2 connections.

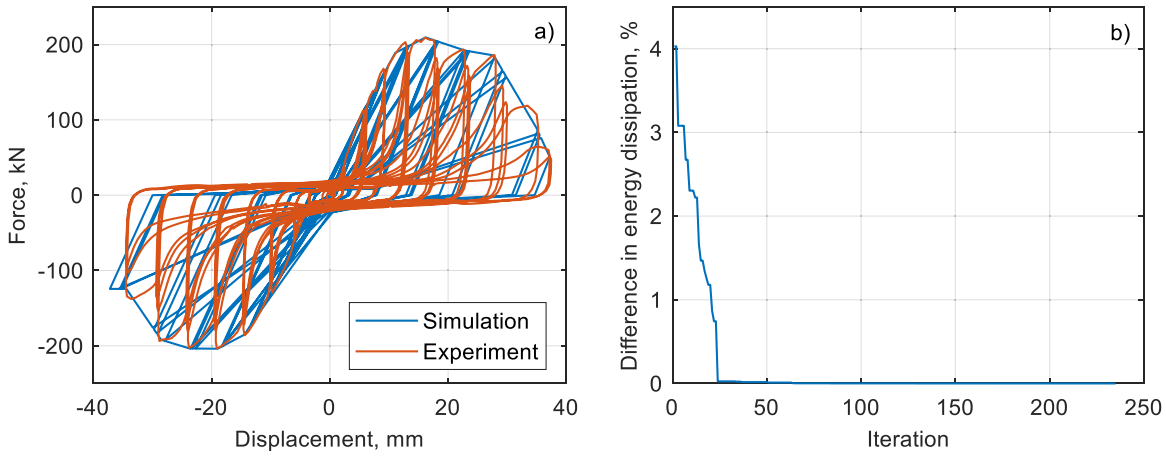

Fig. 14. Performance of the calibration procedure for BC1 connection.

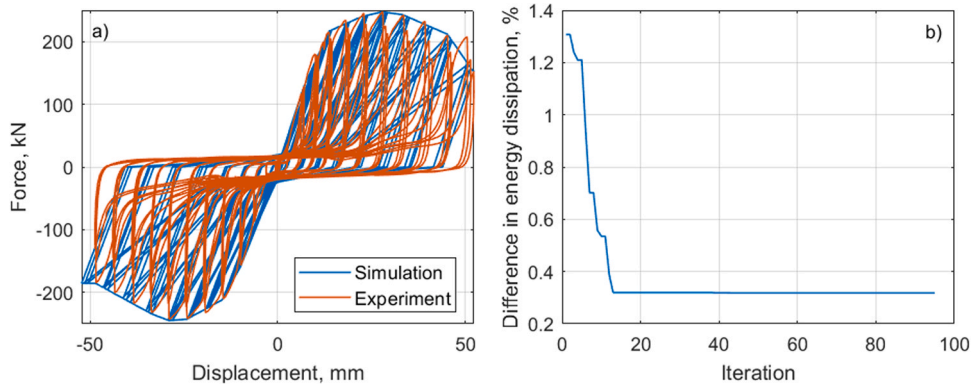

Fig. 15. Performance of the calibration procedure for BC2 connection.

the *HystereticSM* material model to follow the envelope of the hysteresis loops from experimental tests for the two bolted connections considered.

In terms of energy dissipation, the differences are again minimal, as shown in Fig. 14b and Fig. 15b. Specifically, the energy dissipation values for BC1 are 44,800.58 kJ and 44,800.72 kJ for the experiment and simulation, respectively. For BC2, the values are 95,819.12 kJ and 95,818.87 kJ. These observations confirm that the GA effectively optimizes the parameters based on energy dissipation for these two bolted connections.

4.3. Nailed connection

A nailed connection adopted from Qiang et al. [48] was considered for this investigation. The tested nail measured 63.5 × 3.33 mm and was used to connect 15 mm oriented strand board (OSB) panel, to 38 mm x 89 mm No. 2 grade Douglas fir lumber. Connection specimen details are presented in Fig. 16.

Fig. 17a presents the initial selected force-displacement values, and Fig. 17b displays the loading protocol applied to the numerical model and experiment. The loading protocol was generated based on the

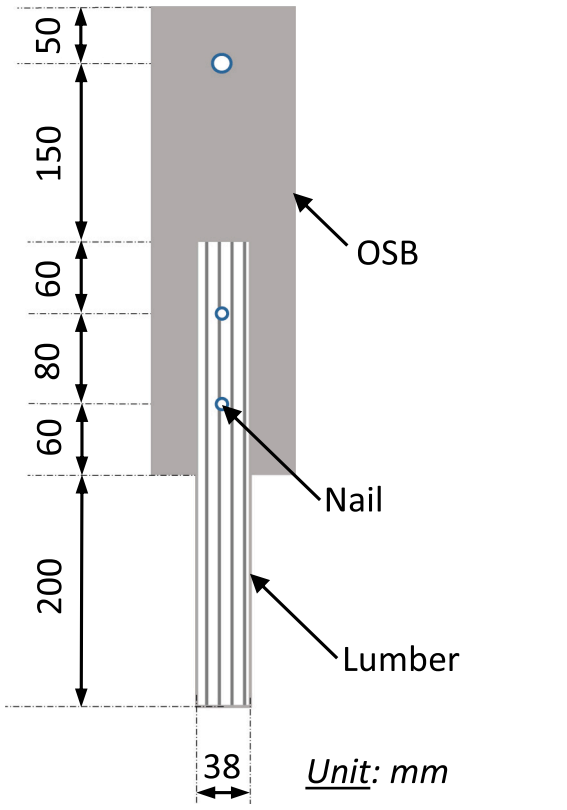

Fig. 16. Specimen configurations of the nailed connection [48].

information provided in [48], which follows Method C of ASTM E2126 [49], using a reference displacement of 31.75 mm (1.25 in.).

The performance of the proposed procedure for the nail connection is illustrated in Fig. 18. In terms of total energy dissipation, both the simulation and experiment produced the same value of 599.06 kJ. The peak force errors between the two models were 0.84 % on the positive side and 0.22 % on the negative side. Overall, the calibration procedure can still yield an acceptable hysteresis loop for the considered nail connection compared to the experiment, despite some discrepancies when the nail connection began to fail. In fact, as shown in Fig. 18a, the nail connection failed during the final loading cycles of the experiment, which led to deviations between the experimental and simulated results, especially in the negative direction.

4.4. Light wood-frame shear wall

For the light wood-frame shear wall, the test data obtained by FPInnovations and the University of Victoria [50] were used for calibration. The shear wall was fabricated with 9.5 mm thick OSB sheathing panels and 63.5 × 3.33 mm diameter nails at spaced at 75 mm at panel edges. Each wall measured 2440 × 2440 mm (8 × 8 feet) with details shown in Fig. 19. The wall was sheathed on one side with two vertically OSB panels. Additional details about the tested wall can be found in the literature [50], where it is referred to as “Wall 2b”.

The initial load-displacement values and the displacement protocol are presented in Fig. 20a and b, respectively. In this calibration, the loading protocol was generated following Method C of ASTM E2126 [49] with a reference displacement of 63.5 mm (2.5 in.).

Fig. 21 shows the performance of the calibration procedure for the light wood-frame shear wall. The peak force on the positive side of the calibrated model is 75.94 kN, corresponding to differences of 0.51 % compared to the experimental result. On the negative side, the differences in peak force between the experiment and simulation are 0.36 %. As shown in Fig. 21b, the calibration procedure stops at iteration 168, with the difference in energy of 0.0005 % between the numerical model and the experiment. In this case, the energy dissipations are 29,114.05 kJ in the experiment and 29,114.19 kJ in the simulation. Generally, the calibrated *HystereticSM* material model successfully produces a hysteresis loop that closely matches the experimental results for the light wood-frame shear wall.

Overall, across four application cases, the outstanding performance of the GA to optimize the energy dissipation in the proposed procedure suggests that the recommended input parameters listed in Table 1 are effective and can serve as a reliable starting point for future applications. However, despite the very small discrepancies in energy dissipation between the experimental and simulated hysteresis loops, further improvements are still needed to better align the loops with the loading path in each cycle, especially in the bolted connections.

5. Conclusions

This study proposes a novel procedure to automate the calibration of the hysteresis loops of timber components using the *HystereticSM* material model. The procedure was presented thoroughly in this study to ensure it can be applied to calibrate hysteresis loops with varying characteristics. The *HystereticSM* model was selected for its ability to capture pinching effects, as well as strength and stiffness degradation. Compared to other commonly used material models, it requires fewer input parameters, which facilitates the calibration process. To accelerate optimization, a GA was employed in the calibration procedure using the

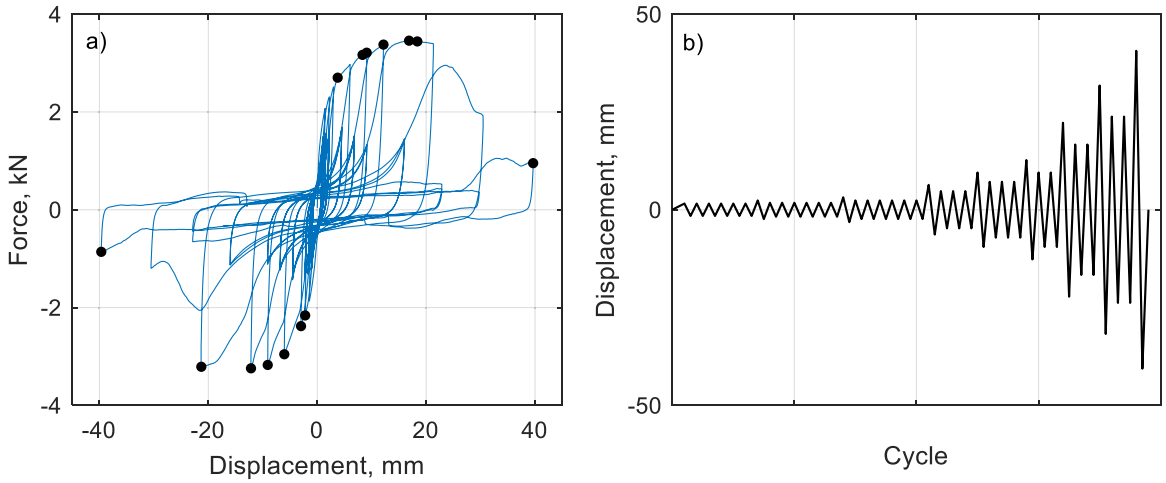

Fig. 17. a) Selected envelope points of force–displacement curve of nailed connection and b) Loading protocol of the experiment.

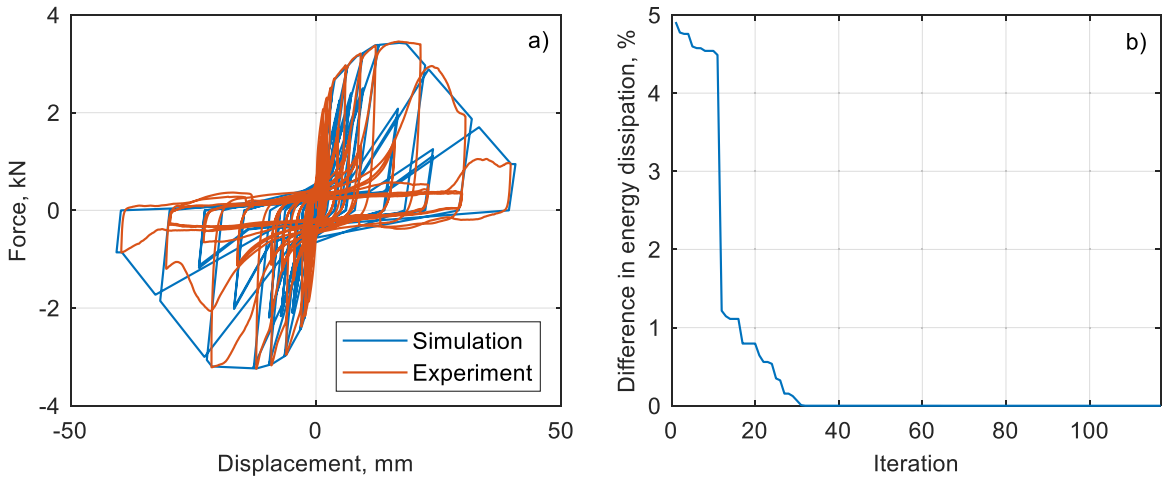

Fig. 18. Performance of the calibration procedure for nailed connection.

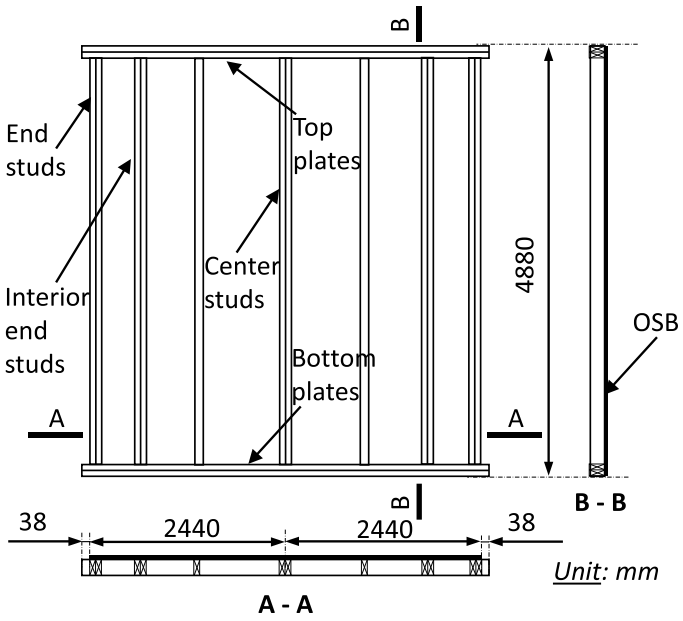

Fig. 19. Experimental setup of light wood-frame shear wall [50].

difference in energy dissipation as the objective function. The proposed procedure was then applied to calibrate hysteresis loops for various types of fasteners in timber connections and light wood-frame shear walls. The investigation has yielded the following conclusions:

- The proposed procedure generally reproduced the hysteresis loops of three types of fasteners (i.e., rivets, bolts, and nails) in timber connections and light wood-frame shear walls with good accuracy when compared to experimental results. Specifically, the errors in terms of peak force and energy dissipation were considered small.
- The calibrated results of four applications confirmed that the *HysteresticSM* was capable of well capturing the pinching effects, as well as strength and stiffness degradation. Therefore, it could be possibility used for different hysteresis behaviors.
- In all application cases, the calibrated models were able to accurately capture the backbone curves, closely matching those obtained from tests. This emphasizes the importance of selecting appropriate initial force-displacement values. Accordingly, the proposed approach for automatically selecting these values proved to be effective.
- For the pinching, beta, damage, and degradation parameters, the initial values should be selected based on the hysteresis characteristics, using the reference values from the parametric study presented in Section 2.2. In this study, the values were set to 0.8 for $pinchx and 0.2 for $pinchy and other parameters ($damage1, $damage2, $beta, $degEnvP and $degEnvN) were initialized at 0.001.

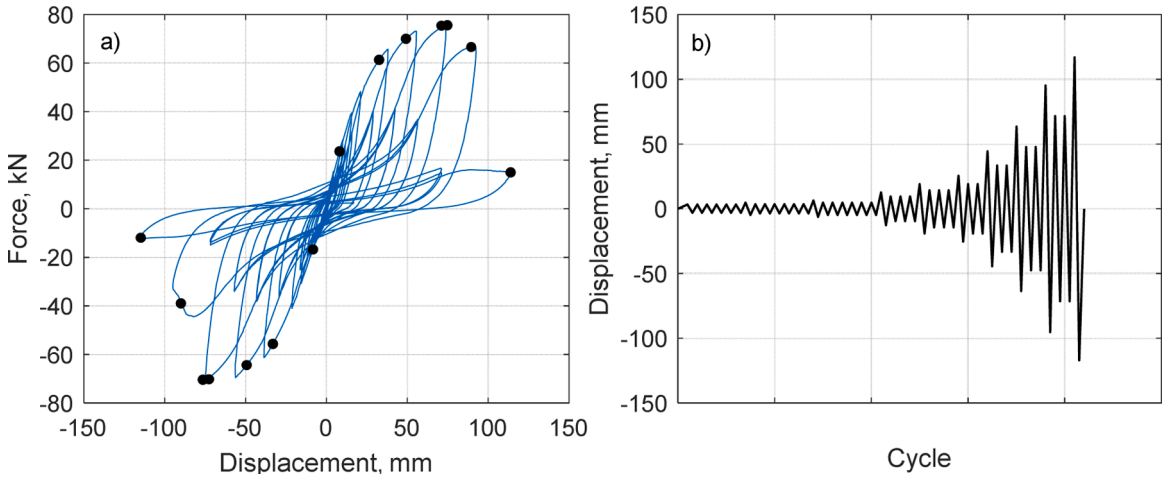

Fig. 20. a) Selected envelope points of force-displacement curve of light wood-frame shear wall and b) Loading protocol of the experiment.

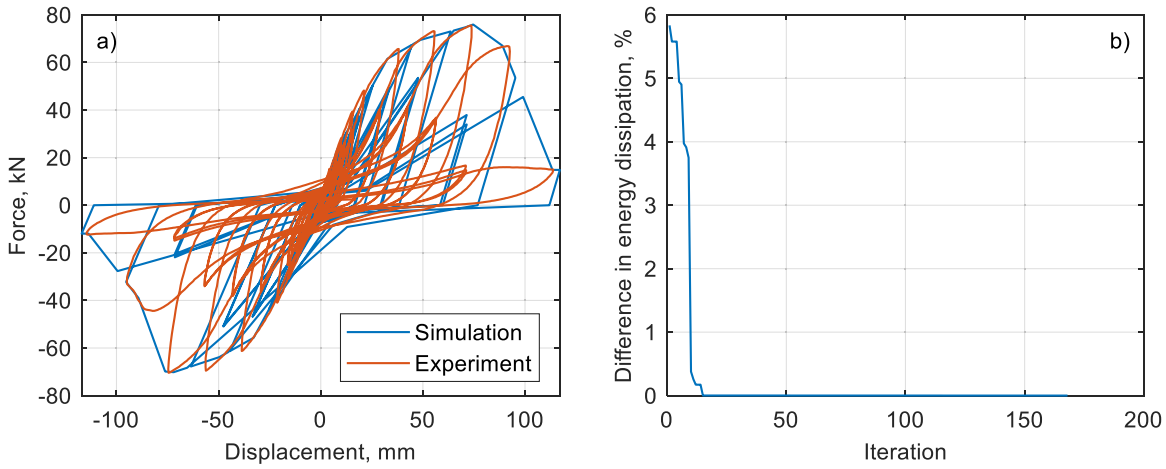

Fig. 21. Performance of the calibration procedure for light wood-frame shear wall.

- The strong performance of the proposed procedure in optimizing the difference in energy dissipation confirms the effectiveness of GA. Furthermore, the use of the 'max_iteration_without_improv' parameter is highly recommended in GA, as it allows the procedure to terminate when no further improvement is observed, thereby reducing overall computational cost.
- Despite the very small discrepancies in energy dissipation and peak force between the experimental and simulated hysteresis loops across four applications, further improvements for the proposed procedure are still needed to better align the loops with the loading path in each cycle.

In this study, the proposed procedure demonstrated strong performance in modeling the hysteresis behavior of timber connections and components. It can be extended to other materials and various types of hysteresis loops/loading protocols to further validate its applicability. In addition, alternative parameters can be considered in the objective function of GA to better align the hysteresis loops with the loading path in each cycle. Furthermore, the influence of parameter bound settings on the numerical adjustment process (e.g., the effect of different bound ranges on the spacing between input values) was not investigated in this work. These directions will be explored in future studies.

CRediT authorship contribution statement

Ying Hei Chui: Writing – review & editing, Validation, Supervision, Methodology, Funding acquisition, Conceptualization. **Qipei Mei:** Writing – review & editing, Supervision, Methodology, Funding acquisition, Validation. **Hoang D. Nguyen:** Writing – original draft, Validation, Methodology, Investigation, Data curation, Conceptualization.

Declaration of Competing Interest

This manuscript has not been published or presented elsewhere in part or in entirety and is not under consideration by another journal. We have read and understood your journal's policies, and we believe that neither the manuscript nor the study violates any of these. There are no conflicts of interest to declare.

Acknowledgement

The authors would like to acknowledge the funding support provided by Natural Sciences and Engineering Research Council (NSERC) of Canada through its Alliance Grant program (Grant number ALLRP 581074–22 and Grant number ALLRP 571090–2), Construction Innovation Centre of the University of Alberta and Alberta Innovates through its Bioindustrial Materials program (Grant number 212201668).

APPENDIX A. INPUT PARAMETERS FOR GA

Parameter	Description	Range
'max_num_iteration'	The stopping criterion for the genetic algorithm. The algorithm terminates when the maximum number of iterations is reached.	[0,∞]
'population_size'	Defines the number of candidate solutions (individuals) in each generation of the population. A larger population increases diversity but requires more computational resources.	[0,∞]
'mutation_probability'	Specifies the probability that a gene in an individual solution will be randomly altered to introduce genetic diversity. Higher values increase exploration but may disrupt good solutions.	[0,1]
'elit_ratio'	Determines the proportion of the population preserved as elites, meaning the best-performing individuals are carried over to the next generation without modification. For example, with a population size of 100 and 'elit_ratio' = 0.01, one elite individual is retained.	[0,1]
'crossover_probability'	Defines the likelihood that two selected parents will exchange genetic material to produce offspring. Higher values promote exploration, while lower values preserve existing solutions.	[0,1]
'parents_portion'	Specifies the fraction of the population that consists of individuals carried over from the previous generation (parents). The remaining portion is filled with newly generated offspring	[0,1]
'crossover_type'	Determines the method of crossover used to combine genetic material from parents.	"one_point", "two_point", and "uniform"
'max_iteration_without_improv'	Defines the number of consecutive iterations without improvement in the objective function before the algorithm stops early. If the best solution remains unchanged over this threshold, the algorithm terminates before reaching 'max_num_iteration'.	"None" or positive integer. Note that it should be less than 'max_num_iteration'

APPENDIX B. INFORMATION OF HYSTERETICSM MATERIAL MODEL

Number of input	Notation	Description
1	$s1p $e1p, …, $s7p $e7p	Force-displacement (or stress-strain; moment-rotation; moment-curvature) values from the first ($s1p $e1p) to the seventh ($s7p $e7p) points defining the envelope in the positive direction.
2	$s1n $e1n, …, $s7n $e7n	Force-displacement (or stress-strain; moment-rotation; moment-curvature) values from the first ($s1n $e1n) to the seventh ($s7n $e7n) points defining the envelope in the negative direction.
3	$pinchx and $pinchy	Pinching factors for strain ($pinchx) and stress ($pinchy) during reloading.
4	$damage1 and $damage2	Factors accounting for damage related to ductility ($damage1) and energy dissipation ($damage2).
5	$beta	Factor determining degraded unloading stiffness based on ductility.
6	$degEnvP and $degEnvN	Envelope-degradation factors used with damage parameters to degrade the positive ($degEnvP) and negative ($degEnvN) envelopes.

Data Availability

Data will be made available on request.

References

[1] Quaranta G, Demartino C, Xiao Y. Experimental dynamic characterization of a new composite glubam-steel truss structure. J Build Eng 2019;25:100773. https://doi.org/10.1016/j.jobe.2019.100773.

[2] Peñaloza D, Erlandsson M, Berlin J, Wålinder M, Falk A. Future scenarios for climate mitigation of new construction in Sweden: effects of different technological pathways. J Clean Prod 2018;187:1025–35. https://doi.org/10.1016/j.jclepro.2018.03.285.

[3] Kumar V, Lo Ricco M, Bergman RD, Nepal P, Poudyal NC. Environmental impact assessment of mass timber, structural steel, and reinforced concrete buildings based on the 2021 international building code provisions. Build Environ 2024;251:111195. https://doi.org/10.1016/j.buildenv.2024.111195.

[4] Dodoo A, Gustavsson L, Sathre R. Carbon implications of end-of-life management of building materials. Resour Conserv Recycl 2009;53:276–86. https://doi.org/10.1016/j.resconrec.2008.12.007.

[5] Younis A, Dodoo A. Cross-laminated timber for building construction: a life-cycle-assessment overview. J Build Eng 2022;52:104482. https://doi.org/10.1016/j.jobe.2022.104482.

[6] Duan Z, Huang Q, Zhang Q. Life cycle assessment of mass timber construction: a review. Build Environ 2022;221:109320. https://doi.org/10.1016/j.buildenv.2022.109320.

[7] Frühwald Hansson E. Analysis of structural failures in timber structures: typical causes for failure and failure modes. Eng Struct 2011;33:2978–82. https://doi.org/10.1016/j.engstruct.2011.02.045.

[8] Frühwald E., Serrano E., Toratti T., Emilsson A.T.S. Design of safe timber structures-How can we learn from structural failures in concrete, steel and timber? Lund University; 2007.

[9] Guo C, Zhou J, Chui YH. Experimental and numerical investigations on vibration performance of mass timber slab floors with floating concrete toppings. Eng Struct 2025;330:119919. https://doi.org/10.1016/j.engstruct.2025.119919.

[10] Zhang S, Chui YH. Quantifying the effect of end support restraints on vibration serviceability of mass timber floor systems: testing. Eng Struct 2024;301:117189. https://doi.org/10.1016/j.engstruct.2023.117189.

[11] Chen Z, Popovski M. Mechanics-based analytical models for balloon-type cross-laminated timber (CLT) shear walls under lateral loads. Eng Struct 2020;208:109916. https://doi.org/10.1016/j.engstruct.2019.109916.

[12] Zhang L, Zhou J, Chui YH, Li G. Vibration performance and stiffness properties of mass timber Panel–Concrete composite floors with notched connections. J Struct Eng 2022;148. https://doi.org/10.1061/(ASCE)ST.1943-541X.0003450.

[13] Mazzoni S, McKenna F, Scott MH, Fenves GL. Open system for earthquake engineering simulation (OpenSees). Pacific Earthq Eng Res Cent; 2006.

[14] Nguyen HD, LaFave JM, Lee Y-J, Shin M. Rapid seismic damage-state assessment of steel moment frames using machine learning. Eng Struct 2022;252:113737. https://doi.org/10.1016/j.engstruct.2021.113737.

[15] Nguyen HD, Dao ND, Shin M. Machine learning-based prediction for maximum displacement of seismic isolation systems. J Build Eng 2022;51:104251. https://doi.org/10.1016/j.jobe.2022.104251.

[16] Nguyen HD, Dao ND, Shin M. Prediction of seismic drift responses of planar steel moment frames using artificial neural network and extreme gradient boosting. Eng Struct 2021;242:112518. https://doi.org/10.1016/j.engstruct.2021.112518.

[17] Nguyen HD, Kim C, Lee K, Shin M. Development of data-driven models to predict seismic drift response of RC wall structures: an application of deep neural networks. Soil Dyn Earthq Eng 2024;186:108952. https://doi.org/10.1016/j.soildyn.2024.108952.

[18] Cheshmehkaboodi N, Nguyen DH, Daneshvar H, Chui YH. Software development for Capacity-Based design of timber braced frames: methodology and performance evaluation. Proc. 14th World Conf. Timber Eng. (WCTE 2025). Brisbane, Australia: World Conference on Timber Engineering; 2025. p. 1388–97. https://doi.org/10.52202/080513-0170.

[19] Folz B, Filiatrault A. Seismic analysis of woodframe structures. Ii: model implementation and verification. J Struct Eng 2004;130:1361–70. https://doi.org/10.1061/(ASCE)0733-9445(2004)130:9(1361).

[20] Folz B, Filiatrault A. Cyclic analysis of wood shear walls. J Struct Eng 2001;127:433–41. https://doi.org/10.1061/(ASCE)0733-9445(2001)127:4(433).

[21] Lowes, L.N., N. Mitra and AA A beam-column joint model for simulating the earthquake response of reinforced concrete frames. Berkeley, CA, 2003.

[22] Shen Y-L, Schneider J, Tesfamariam S, Stiemer SF, Mu Z-G. Hysteresis behavior of bracket connection in cross-laminated-timber shear walls. Constr Build Mater 2013;48:980–91. https://doi.org/10.1016/j.conbuildmat.2013.07.050.

[23] Schneider J, Shen Y, Stiemer SF, Tesfamariam S. Assessment and comparison of experimental and numerical model studies of cross-laminated timber mechanical connections under cyclic loading. Constr Build Mater 2015;77:197–212. https://doi.org/10.1016/j.conbuildmat.2014.12.029.

[24] Cao J, Xiong H, Chen J. Mechanical performance of timber-concrete bolted connections under cyclic loading. Structures 2021;34:3464–77. https://doi.org/10.1016/j.istruc.2021.09.086.

[25] Morshedi E, Doudak G, Fazileh F, Fathi-Fazl R. Seismic performance assessment of wood light-frame shearwalls using the Performance-Based unified procedure. J Struct Eng 2024;150. https://doi.org/10.1061/JSENDH.STENG-13742.

[26] Jerves R, Phillips AR. Cyclic testing and modeling of CLT rocking walls with modular base connections and LSL wall toes. Eng Struct 2024;321:118924. https://doi.org/10.1016/j.engstruct.2024.118924.

[27] Zhu M, McKenna F, Scott MH. OpenSeesPy: python library for the OpenSees finite element framework. SoftwareX 2018;7:6–11. https://doi.org/10.1016/j.softx.2017.10.009.

[28] Chen J, He Z, Wei Y, Wang R, Furuta T, Xiong H. Seismic performance of CLT shear walls anchored with energy-dissipation connections: experimental investigation and parametric analysis. Eng Struct 2025;331:120011. https://doi.org/10.1016/j.engstruct.2025.120011.

[29] Vaiana N, Rosati L. Classification and unified phenomenological modeling of complex uniaxial rate-independent hysteretic responses. Mech Syst Signal Process 2023;182:109539. https://doi.org/10.1016/j.ymssp.2022.109539.

[30] Vaiana N, Rosati L. Analytical and differential reformulations of the Vaiana–Rosati model for complex rate-independent mechanical hysteresis phenomena. Mech Syst Signal Process 2023;199:110448. https://doi.org/10.1016/j.ymssp.2023.110448.

[31] Wu Y, Song X, Ventura C, Lam F. Modeling hysteretic behavior of lateral Load-Resisting elements in traditional Chinese timber structures. J Struct Eng 2020;146. https://doi.org/10.1061/(ASCE)ST.1943-541X.0002613.

[32] Mazzoni S., Scott M.H. Efficient Concentrated-Plasticity Modeling in OpenSees. Proc. 18th World Conf. Earthq. Eng. (WCEE 2024), Milan, Italy; 2024.

[33] Chwastek K, Szczyglowski J. Identification of a hysteresis model parameters with genetic algorithms. Math Comput Simul 2006;71:206–11. https://doi.org/10.1016/j.matcom.2006.01.002.

[34] Di Benedetto S, Latour M, Rizzano G. Cyclic modelling of T-joints with CHS chord members and passing-through plates. Thin-Walled Struct 2024;201:112009. https://doi.org/10.1016/j.tws.2024.112009.

[35] Shi D, Xu Y, Demartino C, Xiao Y, Spencer BF. Cyclic behavior of laminated bio-based connections with slotted-in steel plates: genetic algorithm, deterministic neural network-based model parameter identification, and uncertainty quantification. Eng Struct 2024;310:118114. https://doi.org/10.1016/j.engstruct.2024.118114.

[36] Dong H, He M, Wang X, Christopoulos C, Li Z, Shu Z. Development of a uniaxial hysteretic model for dowel-type timber joints in OpenSees. Constr Build Mater 2021;288:123112. https://doi.org/10.1016/j.conbuildmat.2021.123112.

[37] Wei K, Xu Y. Hysteretic model and parameter identification of RC bridge piers based on a new modified Bouc-Wen model. Structures 2022;43:1766–77. https://doi.org/10.1016/j.istruc.2022.07.049.

[38] Holland JH. Genetic algorithms and the optimal allocation of trials. SIAM J Comput 1973;2:88–105. https://doi.org/10.1137/0202009.

[39] Slowik A, Kwasnicka H. Evolutionary algorithms and their applications to engineering problems. Neural Comput Appl 2020;32:12363–79. https://doi.org/10.1007/s00521-020-04832-8.

[40] Marzocchi A.L. geneticalgorithm: A Python implementation of a genetic algorithm 2018.
[41] Alam T, Qamar S, Dixit A, Benaida M. Genet Algorithm Rev Implement Appl 2020.
[42] Katoch S, Chauhan SS, Kumar V. A review on genetic algorithm: past, present, and future. Multimed Tools Appl 2021;80:8091–126. https://doi.org/10.1007/s11042-020-10139-6.
[43] American Society of Civil Engineers. Seismic evaluation and retrofit of existing buildings. Reston, VA: American Society of Civil Engineers; 2023. https://doi.org/10.1061/9780784416112.
[44] Edelsbrunner H, Kirkpatrick D, Seidel R. On the shape of a set of points in the plane. IEEE Trans Inf Theory 1983;29:551–9. https://doi.org/10.1109/TIT.1983.1056714.
[45] Dokmanic I., Parhizkar R., Ranieri J., Vetterli M. Euclidean Distance Matrices: Essential Theory, Algorithms and Applications; 2015. doi:10.1109/MSP.2015.2398954.
[46] Popovski M., Symons P.D. Structural systems with riveted connections for non-residential buildings. Vancouver, British Columbia; 2003.
[47] Chen Z., Popovski M., Symons P.D. Solutions for Upper Mid-Rise and High-Rise Mass Timber Construction: Seismic Performance of Braced Mass Timber Frames, Year 1. Canada: 2019.
[48] Qiang R, Zhou L, Ni C, Huang D. Reversed cyclic testing of high-capacity light wood frame shear walls with two and three rows of nails. Eng Struct 2024;304:117582. https://doi.org/10.1016/j.engstruct.2024.117582.
[49] ASTM International. ASTM E2126-19: Standard Test Methods for Cyclic (Reversed) Load Test for Shear Resistance of Vertical Elements of the Lateral Force Resisting Systems for Buildings; 2019. doi:10.1520/E2126-19.
[50] Derakhshan SS, Ni C, Zhou L, Qiang R, Huang D. Cyclic test and seismic equivalency evaluation of high-capacity light Wood-Frame shear walls for midrise buildings. J Struct Eng 2022;148. https://doi.org/10.1061/(ASCE)ST.1943-541X.0003448.